Phase-separation and mixing in thin films of co-deposited rod-like conjugated molecules†‡

Jörn-Oliver Vogel,[a] Ingo Salzmann,[a] Steffen Duhm,§[a] Martin Oehzelt,[b] Jürgen P. Rabe[a] and Norbert Koch*[a]

Received 5th January 2010, Accepted 11th February 2010
First published as an Advance Article on the web 23rd March 2010
DOI: 10.1039/b927594k

We report on the formation of organic-organic thin film heterostructures by co-sublimation, which exhibit either mixing of compounds on the molecular scale or pronounced phase separation into ordered domains on the micrometre scale. The mixed structures may be used as active layers in organic field effect transistors, while phase separation is useful in organic bulk hetero-junction solar cells. Pairs of five rod-like conjugated molecules were co-deposited onto silicon oxide substrates in vacuum. With the five materials: pentacene (PEN), alpha-quaterthiophene (4T), alpha-sexithiophene (6T), *p*-sexiphenyl (6P), and alkyl chain substituted α,ω-dihexylsexithiophene (DH6T), we investigated molecule pairs, which differ in the length of the molecular conjugated core (CC) and the overall molecular length. Material pairs with similarly sized CC, such as 4T/PEN and 6T/6P, showed the formation of ordered layered structures with intimated mixing on a molecular level. On the other hand, pronounced phase separation was observed for material pairs of dissimilar CC lengths, *e.g.* 4T/6T and PEN/DH6T. We propose that this can be generalized as design rule for the formation of either mixed or phase separated co-deposited molecular films.

1. Introduction

The formation of supramolecular structures is a successful strategy of nature for building up structures with multiple functions from non-covalently bound standard building blocks. Examples are light harvesting complexes of plants and bacteria in which chlorophyll molecules fulfil the different tasks of collecting the light (antenna complex) and separating charges (reaction centre)[1,2] depending on their spatial arrangement and their local environment. A cell membrane is another example in which the mixing ratio of two components changes the physical properties of the entire structure. The intercalation of cholesterol into lipid bilayers has two effects: it prevents the hydrocarbon chains of the phospholipids from crystallization and decreases the permeability of the bilayer for small water-soluble molecules by decreasing the flexibility of the hydrocarbon chains.[3]

It should be interesting to utilize similar strategies towards improved *organic electronic* applications by combining different organic molecules, which form structures with desired properties by means of self-organization. In the context of *organic electronics*, organic mixed composites have been mostly reported formed from solution processing[4,5] However, the co-deposition of two organic materials from the gas phase, which offers advantages of solvent-free processing and an easy control of the film thickness, has been reported in very few cases. Such studies were focused on donor/acceptor-type molecular pairs for the application in bulk hetero-junction solar cells[6–9] or light emitting diodes,[10] where pronounced phase separation was often observed.[8,11,12] Recently we have shown the possibility of mutual intercalation of rod-like molecules with appropriate alkyl end-chain modifications. In this previous work[13,14] we have investigated materials that are prototypical in the context of organic electronics, *i.e.*, α-sexithiophene (6T),[15,16] its alkylated analogue α,ω-dihexylsexithiophene (DH6T)[17–20] and *p*-sexiphenyl (6P)[19,21] (chemical structures shown in Scheme 1). We showed that co-deposited DH6T/6T and DH6T/6P thin films grow in layered structures with an especially appealing property, *i.e.*, that the interlayer distance *d* linearly depends on the molecular mixing ratio. However, it could not be revealed if the alkyl end-chain and/or a similar conjugated core (CC) *length* were the necessary prerequisites for the mixing of molecules with different *types* of CC (and thus vastly different electronic properties). To address the first issue it is necessary to co-deposit molecular pairs that have similarly sized CC but different types of monomers and, therefore, different electronic and optical properties. For this purpose we have chosen the two pairs of molecules 4T/PEN and 6T/6P, which resulted in well ordered layered structures with an intimate mixing on a molecular level. To test if a large mismatch of the conjugated core sizes prevents intimate mixing, we chose a material pair with identical monomer units but different CC lengths: 4T/6T and pairs with different CC lengths and monomer units, *i.e.*, 4T/6P, 4T/DH6T, PEN/6T, PEN/6P and PEN/DH6T, which resulted in phase separation. The structural properties of the films were characterized by scanning force microscopy (AFM) and X-ray diffraction (XRD). The local environment of the molecules in the

[a]*Humboldt-Universität zu Berlin, Institut für Physik, Newtonstrasse 15, 12489 Berlin, Germany. E-mail: norbert.koch@physik.hu-berlin.de; Fax: +49 (0)30 2093 7632; Tel: +49 (0)30 2093 7819*
[b]*Johannes Kepler Universität Linz, Altenbergerstr. 69, A-4040 Linz, Austria*

† Electronic supplementary information (ESI) available: The IR spectra of a co-deposited film of DH6T and 6P deposited on SiO2. See DOI: 10.1039/b927594k

‡ This paper contains work as a result of a collaborative research project of the German Science Foundation (DFG Sonderforschungsbereich 448) on "Mesoscopically organized composites"

§ Present Address: Graduate School of Advanced Integration Science, Chiba University, Japan

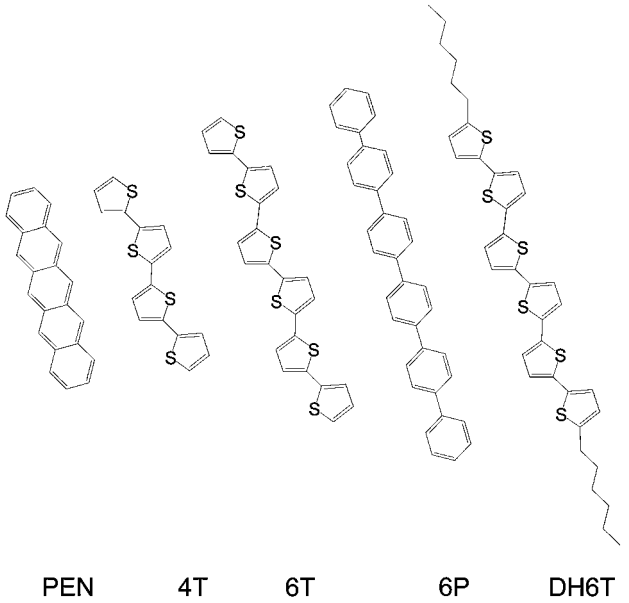

Scheme 1 Chemical structures of the rod-like molecules used in this study: pentacene (PEN), α-quaterthiophene (4T), α-sexithiophene (6T), *p*-sexiphenyl (6P), and α,ω-dihexylsexithiophene (DH6T).

film was probed by infrared absorption spectroscopy (IR). Our data suggest that a match of the CC length leads to mutual intercalation, whereas molecular pairs of differently sized CCs show phase separation. The particular type of conjugated core (*e.g.*, the monomer type) seems not to play an important role for whether intercalation or phase separation occurs.

2. Experimental

Pentacene (Aldrich), 4T (Aldrich), DH6T (H.C. Stark) and 6P (TCI Europe) were used as received. 6T (Aldrich) was purified by temperature gradient vacuum sublimation prior to use. Si (100) coupons of 0.5 and 1.5 mm thickness covered with native oxide (RMS roughness of 0.2 nm, determined by AFM) were used as substrates. The films were deposited by organic molecular beam deposition (OMBD) at room temperature and at a pressure of 3×10^{-7} mbar from two thermal sublimation sources. We measured the deposition rates online *via* a microbalance. Using a shutter, we shadowed one of the deposition sources, allowing us to measure the deposition rates of the individual materials. The mixing ratio values provided below represent the molar ratios in the film. We kept the total deposition rate constant at 0.5 nm min^{-1} and the nominal mass thicknesses of the samples ranged from 1.2 nm–40 nm. X-ray diffraction (XRD) measurements were performed at the beamline W1 at the synchrotron radiation source HASYLAB (Hamburg, Germany) using a wavelength of 0.11808 nm and on a Philips MRD four-circle goniometer with Cu-Kα radiation. All atomic force microscopy measurements were performed with a Veeco Nanoscope III in the tapping mode. The step heights of the layered structures were analyzed as described previously.[13] Infrared absorption spectra (2 cm^{-1} resolution) were obtained on 1.5 mm thick SiO_2 substrates with a Bruker IFS-66v.

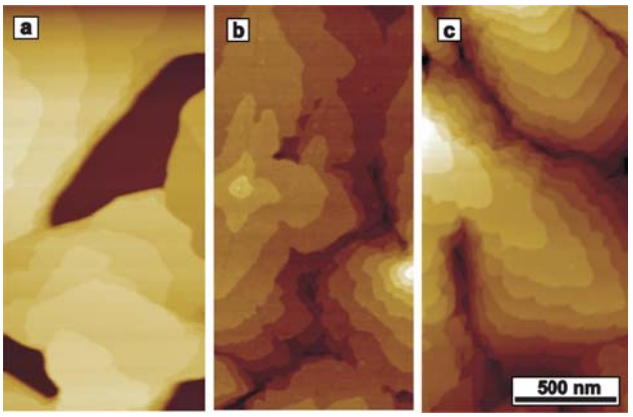

Fig. 1 AFM images of 20 nm thick films. (a) 4T, (b) co-deposited 4T/PEN with 42% 4T and (c) PEN. The measured step heights *d* are 1.50 ± 0.06 nm (4T), 1.56 ± 0.06 nm (4T/PEN), and 1.51 ± 0.06 nm (PEN).

3. Results and discussion

3.1 α-Quaterthiophene/pentacene

The van der Waals lengths (vdWL) of 1.82 nm (4T)[22] and 1.64 nm (PEN)[23] differ by 0.18 nm (10%), calculated from reported crystal structures taking into account a hydrogen van der Waals radius of 0.12 nm. On insulators, both molecules exhibit a well-known thin film growth behavior of layered structures with the long molecular axis standing almost perpendicular to the substrate surface. This can be seen in the AFM height image of 4T film (Fig. 1a) growing in the Volmer-Weber (island) growth mode with well separated islands[24] and PEN (Fig. 1c) growing in the layer-plus-island mode.[25]

Remarkably, the co-deposited 4T/PEN film (Fig.1b) also shows a layered surface morphology. The surface is less corrugated due to the presence of fewer stacked island-layers (~7 layers) compared to the pure 4T (~13 layers) and PEN (~12 layers) films (nominal thickness: 20 nm for all films). No phase separation into individual material domains can be observed *via* AFM for mixing ratios of 11% to 90% 4T.

The average interlayer step height *d* measured by AFM is the same (in the error margin) for the mixed film 1.56 ± 0.06 nm, the pure 4T 1.50 ± 0.06 nm, and PEN 1.51 ± 0.06 nm films. In order to probe the bulk interlayer spacing of the films, specular X-ray diffraction scans (Fig. 2) were performed on the pure materials and co-deposited 4T/PEN samples. The specular XRD scan of the pure 4T film exhibits peaks at values of q_z = 0.4083 $Å^{-1}$, q_z = 0.8233 $Å^{-1}$ and q_z = 1.2196 $Å^{-1}$ vertical momentum transfer, which we assign to the (0 0 *l*) reflections of a polymorph with $d = 1.53 \pm 0.01$ nm, *i.e.*, to the LT-4T[26] (low temperature) polymorph. The pure PEN film shows peaks at q_z = 0.4064 $Å^{-1}$, q_z = 0.8138 $Å^{-1}$ and q_z = 1.2196 $Å^{-1}$ yielding $d = 1.54 \pm 0.01$ nm. We assign them to the (0 0 *l*) reflections of the TF-PEN[27] (thin film) polymorph. The 4T/PEN co-deposited films with 63% 4T and 30% 4T exhibit peaks at q_z = 0.3913 $Å^{-1}$, q_z = 0.792 $Å^{-1}$ and q_z = 1.1874 $Å^{-1}$. We assign them to the (0 0 *l*) Bragg peaks of a layered structure with $d = 1.59 \pm 0.01$ nm. A 46% 4T film measured *in-house* yielded $d = 1.58 \pm 0.03$ nm (not shown).

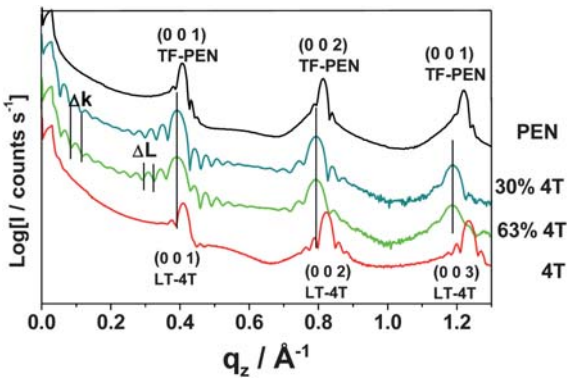

Fig. 2 X-ray diffraction spectra of co-deposited PEN/4T films of 20 nm thickness on SiO_2. Δk is the interval of the Kiessig fringes and ΔL is the interval of the Laue oscillations.

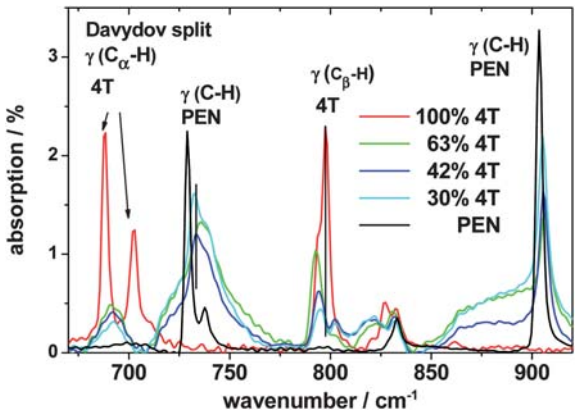

Fig. 3 IR absorption spectra of the γ(C–H) o.-o.-p. bending region of co-deposited 4T/PEN films.

Table 1 Interlayer distance *d* of the 4T/PEN film compared with known PEN and 4T polymorphs. The measured *d* does not coincide with any known 4T and Pentacene polymorph

polymorph	*d*/nm
30%; 63% 4T/PEN	1.59
PEN *Campbell*[30]	1.45
TF-PEN[27,31–33]	1.54
PEN *Holmes*[34]	1.41
PEN *Minakata*[35]	1.50
HT-4T[36]	1.43
LT-4T[36]	1.52

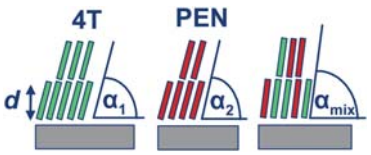

Fig. 4 Increase of the interlayer spacing *d* due to an increase of the tilt angle between long molecular axis and substrate in co-deposited 4T/PEN film. $\alpha_{mix} > \alpha_1, \alpha_2$.

This interlayer spacing is in good agreement with the step height measured by AFM and is, to our knowledge (Table 1), different from all 4T and PEN polymorphs. The existence of Kiessig fringes[28,29] with $\Delta k = 0.0308$ Å^{-1} indicates that the mixed films are less corrugated than the pure 4T and PEN films (also in agreement with AFM data) and have a thickness of 20 nm, which is identical to the nominal mass thickness of the film measured by the microbalance. The Laue oscillations[28,29] with $\Delta L = 0.036$ Å^{-1} indicate that the coherence length of the scattering crystallites is about 18 nm, *i.e.*, it almost equals the nominal film thickness. This indicates that the co-deposited film is of high structural order. We can exclude a phase separation into crystalline compounds because this would result in an overlap of different Bragg peaks, which is not the case. Also a separation into crystalline and amorphous phases would lead to a decrease in the z-extension of the scattering planes.

To gather information on the local environment of the molecules, we performed infrared absorption spectroscopy on the respective films. The IR spectra of the pure 4T film (Fig. 3) shows a Davydov split peak[37] with the two peak maxima centered at 688.1 cm^{-1} and 702.4 cm^{-1}, which is associated with the $\gamma(C_\alpha–H)$ out-of-plane (o.-o.-p.) vibration of the hydrogen atoms at the end-positions of the 4T molecule. In a co-deposited film with 63% 4T, the Davydov splitting vanishes and a single peak occurs centered at 691.9 cm^{-1}. This indicates that the molecular occupation of the crystal unit cell changed significantly. We will show later in this paper that in phase separated films (*i.e.* 4T/DH6T film) the splitting of the Davydov-peaks prevails. The change of the local environment of the 4T molecules is also supported by the 4.6 cm^{-1} red shift of the $\gamma(C_\beta–H)$ vibration at 797.6 cm^{-1} associated with the hydrogen atoms at the β-positions of the 4T thiophene rings.

We will now discuss the peak shifts of the PEN molecules caused by co-deposition with 4T. The γ(C–H) o.-o.-p. vibration[38] of the pure PEN film at 729 cm^{-1} shows strong broadening and a maximal blue shift of 8 cm^{-1} in the 63% 4T film. The increase of the broadening with decreasing PEN content indicates that the local environment of the PEN molecules becomes less homogeneous. This points towards statistical mixing of PEN and 4T molecules in the molecular layers. The blue shift of 2.4 cm^{-1} of the PEN γ(C–H) vibration at 903.5 cm^{-1} is also indicative of the change in the film structure compared to the pure PEN film. These strong changes in the IR spectra for 4T and PEN, together with the finding of layered growth (from AFM and XRD) give strong evidence for an intimate mixing of 4T and PEN on a molecular scale. A collective change of the tilt angle between the long molecular axis and the substrate surface could explain the increase of the interlayer spacing (Fig. 4). This could also point to the conclusion that *d* is independent of the 4T/PEN mixing ratio in the measured range.

3.2 α-Sexithiophene/*p*-sexiphenyl

The vdWL of 6T[39] (2.61 nm) and 6P[40] (2.87 nm) differ by 0.26 nm (9%), the absolute mismatch being 0.1 nm larger than for 4T/PEN. The AFM height image of the 6T/6P film (Fig. 5b) shows layered structures similar to the 4T/PEN films. The pure 6T (Fig. 5a) and 6P films (Fig. 5c) exhibit their typical thin film

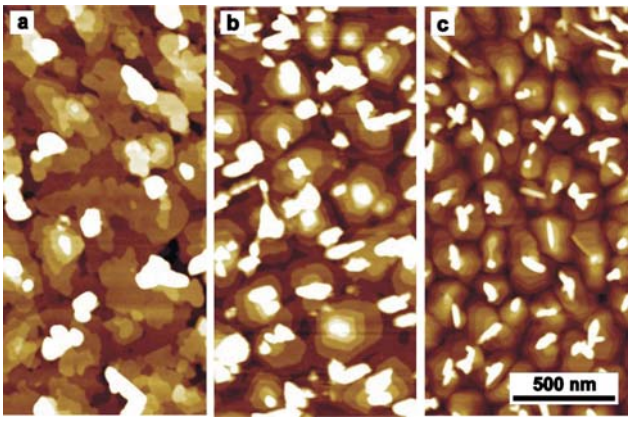

Fig. 5 AFM images of 20 nm thick films deposited on SiO_2. (a) 6T, (b) co-deposited 6T/6P with 43% 6T and (c) 6P. The measured step heights d are 2.19 nm (6T), 2.57 nm (43% 6T) and 2.69 nm (6P).

morphology[39,41] of layered structures. The co-deposited 6T/6P film with a 43% 6T ratio exhibits an island density which is comparable to the 6P film. It is noteworthy that some edges of the islands enclose angles of 120 ± 20°, similar to the angles found for the islands of the pure 6P film. This is an indication that the in-plane-ordering of the co-deposited film may be similar to that of the 6P film.

Next, we discuss the specular XRD scans of the films shown in Fig. 6 starting with the pure 6T film of 40 nm thickness. The 6T film exhibits sharp peaks of a (2n 0 0) series up to $n = 6$ leading to an interlayer spacing of $d = 2.25 \pm 0.05$ nm, that is the LT-6T[42] (low temperature) phase ($d = 2.236$ nm) and γ-6T[43] phase ($d = 2.24$ nm). The series of broad peaks belonging to a spacing of $d = 2.42$ nm represents the β-6T phase[43] (2.44 nm).

The 74% 6T film of 20 nm thickness shows - compared to the pure 6T film - weaker peaks of the (2n 0 0) series of the LT-6T[42] polymorph. We assign the peaks at $q_z = 0.4715$ Å^{-1} and $q_z = 0.728$ Å^{-1}, marked with dashed lines, to contributions of a mixed phase with $d = 2.59 \pm 0.1$ nm.

The 40 nm 58% 6T film exhibits a (h 0 0) series belonging to $d = 2.60 \pm 0.05$. The 52% 6T (30 nm thick) and 42% 6T (20 nm thick) have interlayer spacings of $d = 2.62 \pm 0.05$ nm and $d = 2.66 \pm 0.05$ nm. The specular scan of a 26% 6T film (40 nm thick) (not shown) measured with Cu-Kα radiation resulted in $d = 2.68 \pm 0.05$ nm. The pure 6P (10 nm thick) film exhibits regular (0 0 l) peaks with $d = 2.74 \pm 0.05$ nm of the γ-6P[44] phase with $d = 2.72$ nm.

The interlayer spacing d and the step heights on the film surfaces measured by AFM are plotted in dependence of the 6T content in Fig. 7. From 0% 6T to 60% 6T content, d shows a weak monotone decreasing dependence on the mixing ratio. The specular scan of the 74% 6T film shows the co-existence of a pure LT-6T phase and a mixed phase. We measured the step heights on individual islands of the 74% 6T film *via* AFM. The step heights cumulate at ~2.25 nm which we associate to pure 6T islands and ~2.45 nm associated to the mixed phase which are both observable in the specular XRD scan. Additionally a broad distribution around 2.6 nm is observable which we can associate with 6P rich islands. It is worth mentioning that it is hard to measure the step heights of individual islands because of its small extension.

Additional information about the local environment of the molecules in the film can be derived from IR spectroscopy (Fig. 8). We first address the γ(C–H) o.-o.-p. vibration peaks[45] of the 6P molecules. The γ(C_α–H) vibration of the 6P-end-rings at 760 cm^{-1} exhibits a blue-shift of 3 cm^{-1} with increasing 6T content. The γ(C_p–H) vibration of the *para*-substituted rings shows a comparable blue shift (2.9 cm^{-1}) from 814.2 cm^{-1} (6P) to 817.1 cm^{-1} (74% 6T) film.

Remarkably, the γ(C_β–H) vibration peak[46] of the 6T molecule at 791.6 cm^{-1} loses its fine structure when a small amount of 6P is

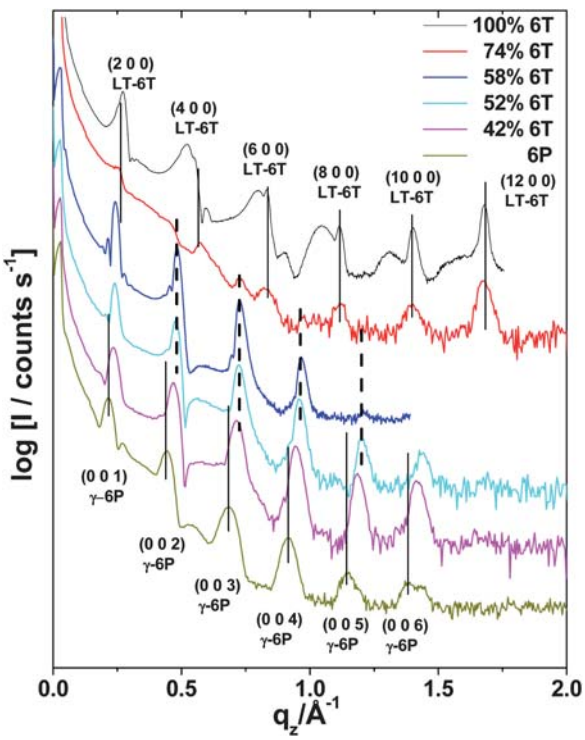

Fig. 6 Specular X-ray diffraction scans of co-deposited 6T/6P film. The thin solid lines mark the peaks of the (2n 0 0) series of the LT-6T (low temperature) polymorph and the (0 0 l) reflection of the γ-6P polymorph. The dashed line marks the peaks of mixed crystal polymorphs.

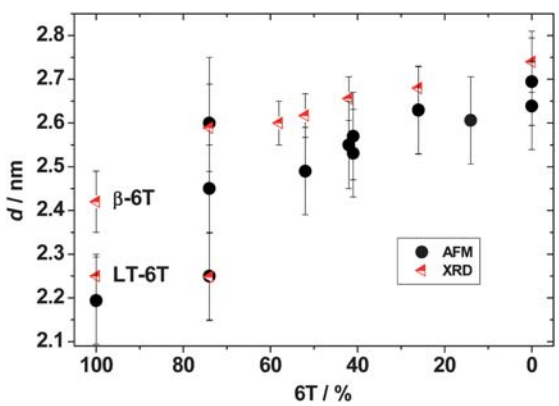

Fig. 7 Interlayer distance d of co-deposited 6P/6T films measured by AFM and XRD as a function of the 6T content.

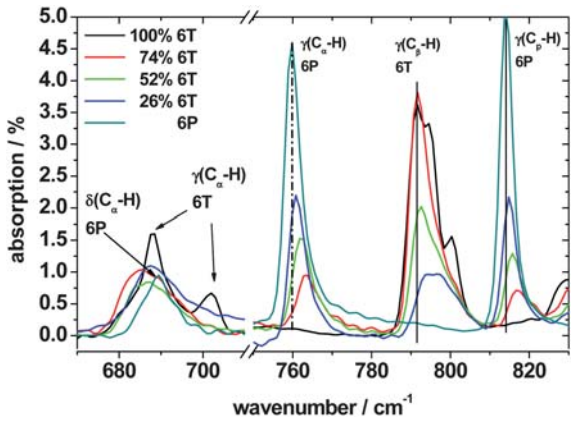

Fig. 8 IR absorption spectra of the γ(C–H) o.-o.-p. bending region of co-deposited 6T/6P films. The absorption is scaled to 40 nm film thickness.

co-deposited. With further increase of the 6P content, this peak shows a pronounced blue shift of 3.4 cm^{-1} (26% 6T).

Of particular importance is the Davydov split[37] 6T γ(C_α–H) o.-o.-p bending peak at 688 cm^{-1} and 702 cm^{-1}. The 74% 6T film shows only a broad peak around 686 cm^{-1}, which is a superposition of the 6P δ(C_α–H) ring deformation vibration peak at 689.5 cm^{-1} and the unsplit broad 6T γ(C_α–H) peak around 682.5 cm^{-1} that was measured earlier for intercalated films of 6T/DH6T. As discussed in Ref. 13 the vanishing of this Davydov splitting indicates that the local environment of 6T molecules changed suddenly due to the co-deposition of 6P. However, it is possible that the IR spectrum of the 74% 6T film may contain a small contribution of the Davydov split 6T γ(C_α–H) peak and is therefore not in contradiction to the detection of pure 6T domains in the 74% 6T film by XRD.

The data suggest that the 6T/6P co-deposited films exhibit coexistence of pure 6T and mixed 6T/6P domains for a high 6T content of >60% 6T (Fig. 9). Since the vdWL of 6P is slightly longer than the vdWL of 6T, intercalation of the smaller 6T molecules into the 6P structure becomes possible, leaving only small holes that do not hamper the growth of the next layer. In the reverse case, a 6P molecule intercalated into a 6T layer would stick out of the 6T surface, since the 6P molecules are forced to exhibit similar orientation to the surrounding 6T molecules, thus hampering the growth of the next 6T layer. This causes the phase separation into pure 6T and 6P rich mixed domains. Therefore, we expect that 6P-rich films will show no phase separation. To further test this model, it is necessary to co-deposit more molecules with different CC lengths, which should result in either a phase separation or an amorphous mixture.

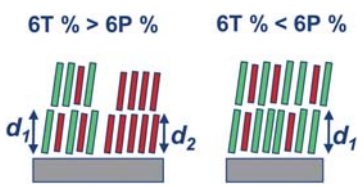

Fig. 9 Cartoon of the mutual molecular arrangement. For 6T rich films we found phase separation into a pure 6T phase (d2) and 6P rich intercalated 6T/6P phase (d1). The 6P rich film did not exhibit phase separation.

3.3 α-Quaterthiophene/α-sexithiophene

To determine if a matching length of the CC is a necessary prerequisite for mixing/intercalation, we co-deposited two materials with the same *type* of CC but different *vdWL*. The vdWL of 4T[22] (1.82 nm) and 6T[39] (2.61 nm) differ by 0.79 nm (30%). The surface of the 20 nm thick co-deposited 4T/6T film with 62% 4T content (Fig. 10) exhibits three different kinds of features: layered structures of 2.3 nm step height (Fig. 10a) covering a small amount of the surface, 1000 nm × 250 nm (typical values) footprint-area islands of 150 nm–200 nm height, and 50 nm high frayed islands (Fig. 10b), plus some small needle-like islands of 40–50 nm height. This complex surface morphology is an first indication, that the 4T/6T sample does not consist of one homogeneous mixed film.

The specular XRD scans, measured with Cu-Kα radiation, are shown in Fig. 11. The scans of the pure material films are shown in Fig. 2 and Fig. 6. The 22% 4T film shows unshifted peaks of the (0 0 2n) series of the LT-6T[42] or γ-6T[43] polymorph, indicating standing molecules. We can identify the peak at $q_z = 1.42$ Å^{-1} as a superposition of the (0 0 10) and (4 1-1) peak of the LT-6T phase. The LT-6T (4 1 −1) and the (0 2 0) at $q_z = 1.599$ Å^{-1} indicate a molecular arrangement almost perpendicular to the substrate surface. Peaks of standing 4T molecules in the LT[36] phase are at $q_z = 0.824$ Å^{-1} (0 0 4) and at $q_z = 1.65$ Å^{-1} (0 0 8). They are superimposed with the LT-6T (0 0 6) and (0 0 12) peaks.

The 53% 4T film exhibits an unshifted (0 0 2n) series of the LT-4T polymorph indicating that the 4T molecules are oriented perpendicular to the substrate surface. We identify the peak at

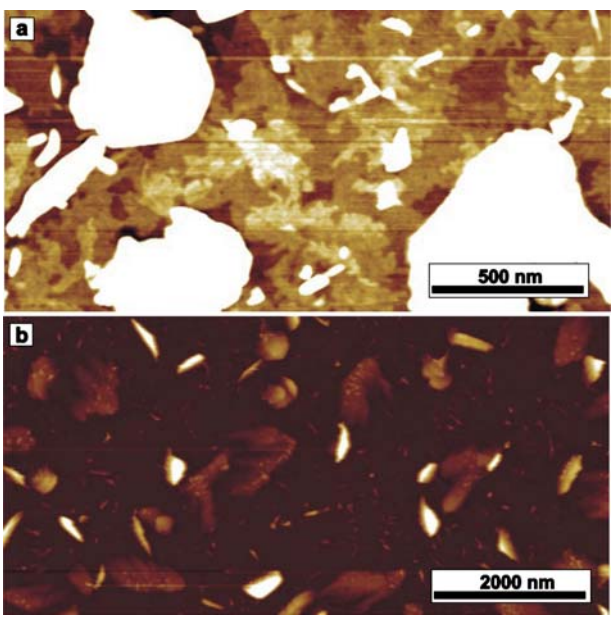

Fig. 10 AFM images of 62% 4T/38% 6T film of 20 nm thickness. (a) Height scaled to show layered structure with 2.3 nm step height, (b) height scaled to show island morphology: high needle-like islands (150–200 nm height), frayed islands (50 nm height) and small needle-like island (40–50 nm height).

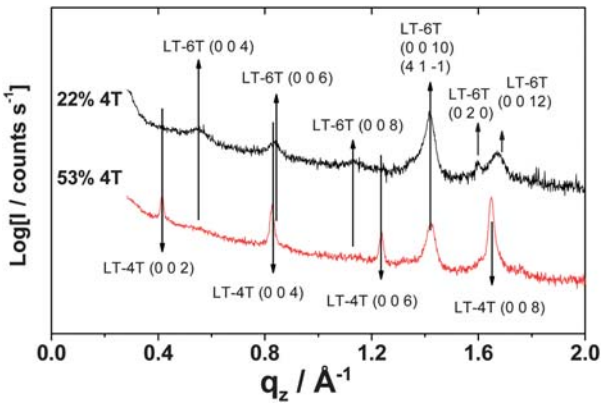

Fig. 11 Specular XRD scans of co-deposited 40 nm thick films of 4T/6T on SiO_2.

$q_z = 1.4231$ Å^{-1} as (4 1 −1) of the LT-6T phase. The XRD data show no sign of a mixed phase of 4T and 6T. The low intensity of the peaks leads to the following possible interpretations: (i) A large amount of 4T and 6T is not ordered and, as a result, causes no diffraction peaks; (ii) The scattering planes are not oriented parallel to the substrate surface and therefore, they cannot be detected in the θ–2θ specular scan.

The amorphous growth assumed in (i) would lead to strong changes in the IR spectra, since the local molecular environment is different for every single molecule as in a solution. Fig. 12 shows that the IR spectra of co-deposited films are simple superpositions of the pure material film spectra. Of special interest is the fact that the Davydov splitting of the $\gamma(C_\alpha$–H) vibration peak of 4T and 6T does not vanish in the co-deposited film. This indicates that the local crystal structure of the 4T and 6T molecule is unchanged in the co-deposited film in contradiction to (i). This supports (ii) which indicates that a larger part of the co-deposited film consists of ordered phase separated domains of 4T and 6T which have no preferential orientation to the substrate surface causing the low scattering intensities (XRD) and "tilted" islands (AFM).

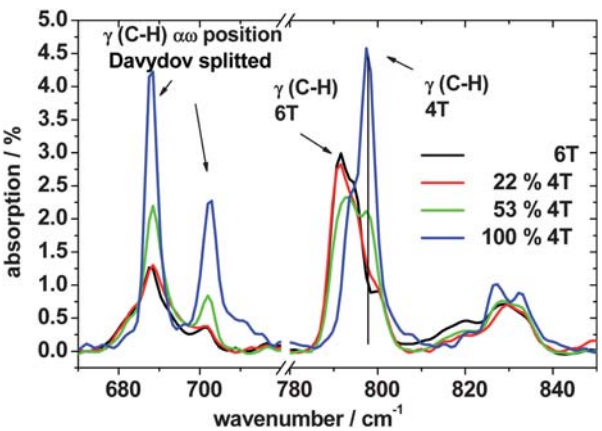

Fig. 12 IR absorption spectra of the γ(C–H) out-of-plane bending region of co-deposited films of 4T/6T. Please note that the mixed film spectra are superpositions of the pure film spectra.

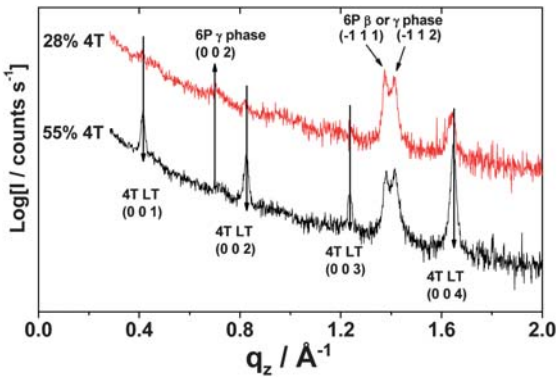

Fig. 13 Specular XRD scan of 40 nm 4T/6P films.

3.4 α-Quaterthiophene/*p*-sexiphenyl

Similarly to the preceding material pair 4T/6T, the vdWL of 4T[22] (1.82 nm) and 6P[40] (2.87 nm) differ by 1.05 nm (37%). The specular XRD scans of the pure 4T and 6P films are shown in Fig. 4 and Fig. 6 for reference. The specular XRD scan (Fig. 13) of the 28% 4T co-deposited film shows a weak peak at $q_z = 0.7023$ Å^{-1} that we assign to (0 0 2) of almost standing 6P molecules in the γ-phase.[44] The standing 4T molecules in the low temperature phase[36] are represented by the (0 0 *l*) series with a pronounced (0 0 4) peak. There are two strong peaks at $q_z = 1.376$ Å^{-1} and $q_z = 1.415$ Å^{-1} that we can assign to (−1 1 1) and (−1 1 2) reflections of the β-phase[40] or γ-phase of 6P[44] and the HT-phase[26]of 4T. This shows that a large number of the molecules are oriented almost parallel to the substrate. In detail, the

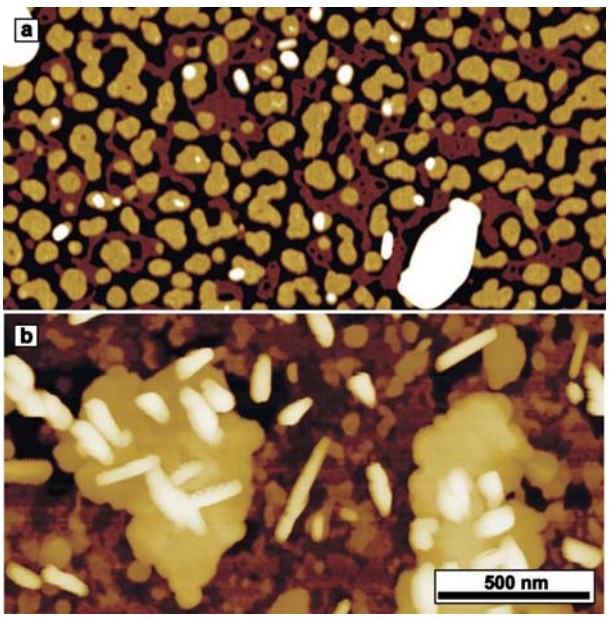

Fig. 14 AFM images of co-deposited films of 4T and 6P grown on SiO_2. (a) 56% 4T film of 4.6 nm thickness. Please note the 30 nm high island and the small holes in the layered structures. (b) 60% 4T film of 20 nm thickness shown in a nonlinear height scale. Note the three different morphologies: Layered structures covering the ground, 40–60 nm high 4T-like islands, and 40–50 nm high needles.

cleavage planes of the crystallites are oriented parallel to substrate.

The 55% 4T film exhibits a more pronounced (0 0 *l*) series of LT-4T[36] and a consequently weaker (0 0 2) peak of the 6P γ-phase. The peaks at $q_z = 1.376$ Å^{-1} and 1.415 Å^{-1} show similar strength, indicating that both 4T and 6P contribute to these peaks.

The AFM height image a 4.6 nm thick 56% 4T film (Fig. 14a) exhibits layered structures with 2.86 nm step height (similar to vdWL of 6P) and "round" island borders. Note the numerous holes in the islands, which could be 4T inclusion in 6P islands. The white spot is a 25 nm high island with no depletion zone around it, indicating that the layered structures and the high islands grow independently. This suggests that 4T separates into the high islands from the first layer on. The surface of a 20 nm thick 60% 4T film (Fig. 14b) exhibits three different features: layered structures covering the substrate that we can relate to the domains of standing 6P, 40 nm high needle-like islands, islands of 60–90 nm height and 500 nm footprint with either flat (standing molecules) or tilted surfaces (lying molecules). We can relate the latter island type to 4T since their number increases with increasing 4T content of the film.

The IR spectra (Fig. 15) show only weak peak shifts of about 0.5 cm^{-1}. As discussed before, the persistence of the Davydov splitting of the 4T γ(C$_\alpha$–H) vibration and the weak blue shifts of the 6P peaks (~0.5 cm^{-1}) in the co-deposited film spectra show that most of the 4T and 6P is in the pure material state which indicates a good phase separation into ordered but not textured 4T and 6P domains.

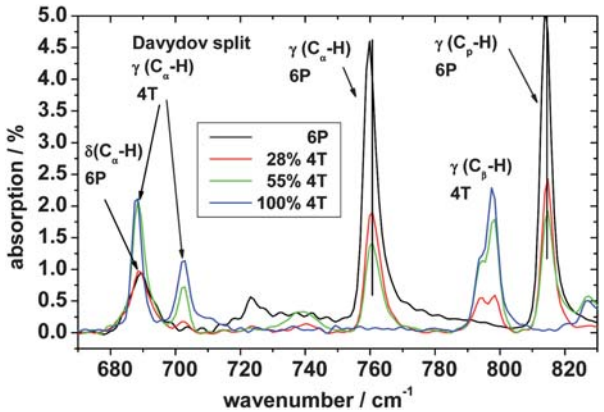

Fig. 15 IR spectrum of co-deposited thin films of 4T/6P of 40 nm thickness. Note that the 4T γ(C$_\alpha$–H) vibration is Davydov split for all 4T contents. All other peaks show only weak blue shifts (~0.5 cm^{-1}).

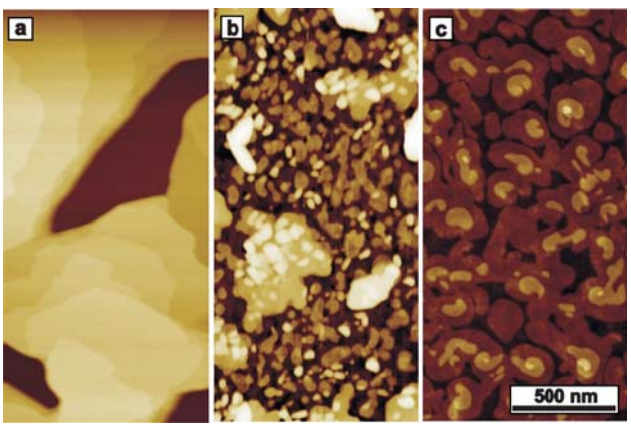

Fig. 16 AFM images of 20 nm nominal thickness. (a) 4T, (b) 53% 4T, (c) DH6T. The co-deposited film (b) is shown with nonlinear height scale to show the DH6T-film-like morphology covering the substrate with ~3.05 nm steps and the 15–150 nm high islands.

3.5 α-Quaterthiophene/α,ω-dihexylsexithiophene

Since 6T/DH6T and 6P/DH6T formed well-ordered, intercalated, layered structures,[13] we could assume that the alkyl-end-substitution promotes the growth of well-ordered mixed structures. We therefore co-deposited 4T and DH6T which have the same CC, just as the phase separating pair 4T/6T. The AFM height image of a 20 nm thick 53% 4T co-deposited film (Fig. 16b) is displayed in a nonlinear height scale to resolve the typical DH6T-like morphology (Fig. 16c) covering the substrate. The DH6T-like film exhibits step heights of about 3 nm, similar to $d = 3.2 \pm 0.2$ nm of the pure DH6T[13] film. The 15 nm–150 nm high islands have a similar shape as 4T films islands (Fig. 16a). The steps on top of the high islands have a height of about 1.5 nm, similar to the $d = 1.50 \pm 0.06$ nm measured for the pure 4T film. This seems to indicate a phase separation into domains of standing 4T and DH6T molecules.

The specular XRD scan (Fig. 17) of the co-deposited films with 80% 4T and 38% 4T exhibits the unshifted (0 0 1) and (0 0 2) peaks of the LT-4T[36] phase. The weak (0 0 2) peak of the HT-4T[26] (high temperature) phase with $d = 1.423$ nm is pronounced in the co-deposited film spectra. The (0 0 1) and (0 0 2) peaks of the DH6T film belonging to $d = 3.64$ nm are present in the co-deposited film scan, though they are of weak intensity and significantly broader which is just an effect of the low effective DH6T film thickness in the co-deposited film. The XRD spectra show no peaks indicating lying molecules (not shown).

The IR spectra of the γ(C–H) o.-o.-p. bending region (Fig. 18) show that the spectra of the co-deposited film are just superpositions of the pure material film spectra. This indicates that phase separation into domains of pure 4T and DH6T occurs. AFM and

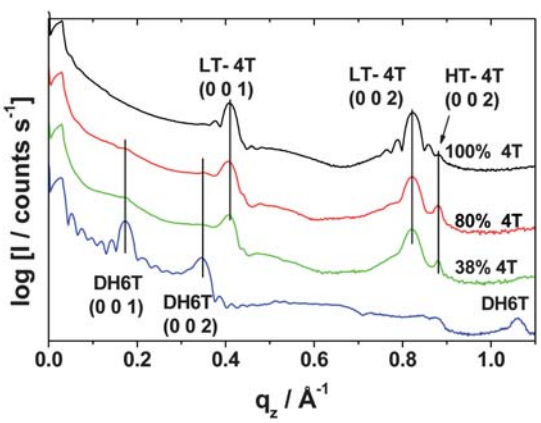

Fig. 17 Specular XRD scans of co-deposited 4T/DH6T films. The thickness of the DH6T film is 40 nm; all other films are 20 nm thick.

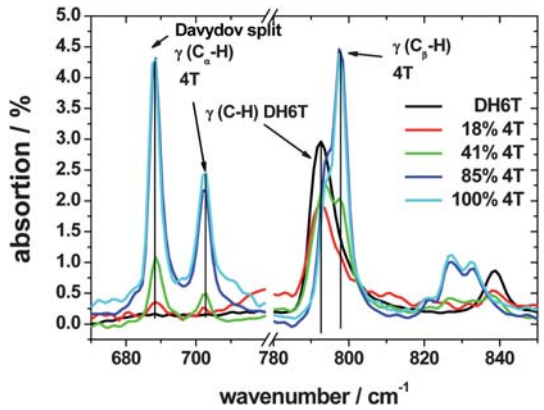

Fig. 18 IR absorption spectra of the γ (C–H) o.-o.-p. bending region of co-deposited films of 4T/DH6T on SiO_2. The mixed film spectra are superpositions of the pure film spectra.

XRD data congruently show that most of the film layers are oriented parallel to the substrate. We therefore conclude that 4T/DH6T films grow in phase separated ordered domains of standing molecules, very similar to the respective pure material films.

3.6 Pentacene/α,ω-dihexylsexithiophene

PEN/DH6T is the most diverse material pair with respect to the vdWL of CC, the monomer type, and the alkyl-chain-substitution. The vdWL of the CCs differ by about 1 nm (40%), with 1.64 nm for PEN[23] and 2.61 nm (DH6T), if 6T[39] is used as reference. The AFM images shown in Fig. 19 depict three films with increasing DH6T content. The substrate is covered in the 26% PEN film (Fig. 19a) with a two layer structure with ~3.1 nm step height, similar to the step height $d = 3.2 \pm 0.2$ nm measured with AFM on pure DH6T[13] films. Additionally the film exposes 10 nm–20 nm high islands. The film with 62% PEN (Fig. 19b) shows 20 nm high islands with very diverse shape and 30 nm high elongated islands. The diverse shape of the islands can be an indication that the islands consist out of different compositions. The 79% PEN, on the other hand, shows interconnected islands of 20 nm height and additional 40 nm high small islands.

The specular XRD scan (Fig. 20) of a pure PEN film shows a series of (0 0 *l*) peaks of the TF-PEN[27] phase. The co-deposition

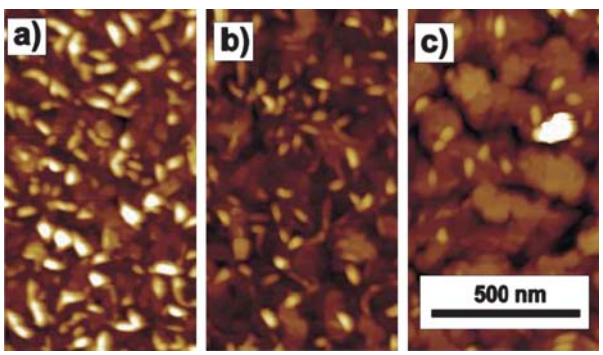

Fig. 19 AFM image of 20 nm thick co-deposited PEN/DH6T films: (a) 26% PEN, (b) 62% PEN and (c) 79% PEN.

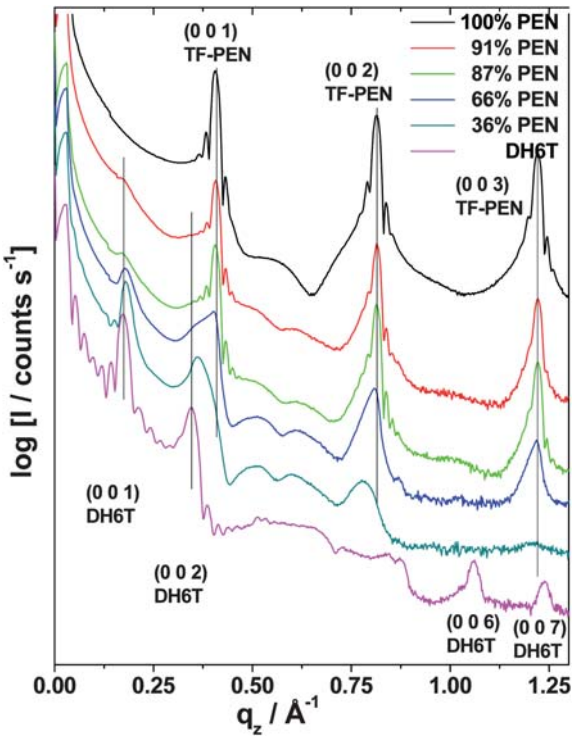

Fig. 20 Specular XRD scans of PEN/DH6T co-deposited films of 40 nm thickness.

of DH6T leads to a weak broad peak at $q_z = 0.1744$ Å^{-1}, which we identify as the (0 0 1) peak of DH6T[13] with $d = 3.6$ nm. As the (0 0 1) peak of the TF-PEN[27] phase and the (0 0 2) peak of DH6T are superimposed at very similar q_z values, it is impossible to identify possible small changes of the interlayer spacing. The peak intensities of the (0 0 1) peaks of PEN and DH6T decreases proportional to PEN/DH6T content in the film. This indicates a phase separation into domains of standing PEN and DH6T molecules.

The IR spectra (Fig. 21) of the DH6T γ(C–H) o.-o.-p. bending vibration peak[36,37] exhibits a negligible blue shift of 1 cm^{-1} compared to 2.5 cm^{-1} for DH6T/6P (SUPPORTING INFO). The PEN γ(C–H) o.-o.-p peak[38] only shifts by 2 cm^{-1} compared to a 5 cm^{-1} shift and the accompanying strong broadening in the mixed film spectra of PEN/4T (Fig. 3). From all these

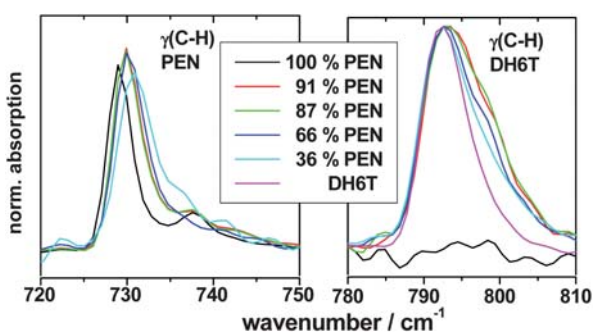

Fig. 21 The γ(C–H) o.-o.-p vibration peaks of PEN and DH6T are normalized to peak maximum.

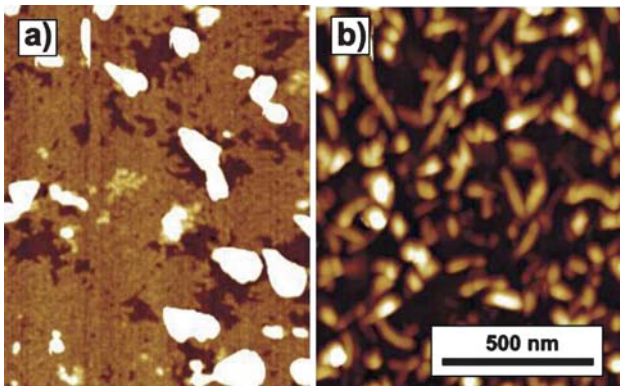

Fig. 22 AFM images of co-deposited PEN/6T films with (a) 55% PEN and 4.7 nm thickness, (b) 46% PEN and 20 nm thickness.

observations we can conclude that PEN and DH6T phase separate into domains of standing PEN and standing DH6T.

3.7 Pentacene/α-sexithiophene

The next material pair, PEN/6T, (vdWL 1.64 nm[23]/2.61 nm[39]) differs from the preceding material pair by the absence of alkyl-chain-substitution on the 6T. The AFM image of a 55% PEN film of 4.7 nm thickness (~2 mono layers) is shown in Fig. 22a. The film consists out of an almost closed first layer with smooth surface. On top of that is a second layer located consisting out of loosely packed islands with a height of 1.6 nm to 2 nm. This height variation already indicates mixing and/or phase separation on the nm scale at least in the second layer. The third distinct height level comprises small islands of typical 10 nm height. It should be mentioned that the loosely packed second layer poses a rough surface for the following molecules. That is different to the phase separating material pairs discussed before which showed pronounced phase separation already in the 1 to 2 monolayer range. The 20 nm thick 46% PEN film (Fig. 22b) exhibits a very high surface corrugation. It consists out of small 30 nm–80 nm high islands with high islands density.

We now turn to the specular XRD scan (Fig. 23) of a 40 nm 45% PEN film. It shows rather broad features. The one at q_z = 0.3037 Å^{-1} (corresponding to d = 2.07 nm) could be the (0 0 1) peak of HT-6T[39] phase (with d = 2.048 nm) or could indicate the

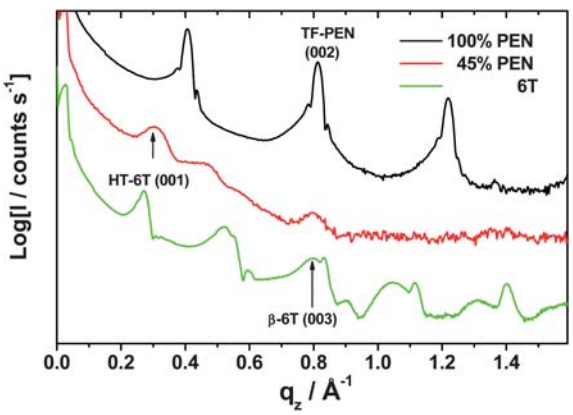

Fig. 23 Specular XRD scans of 40 nm thick PEN/6T film.

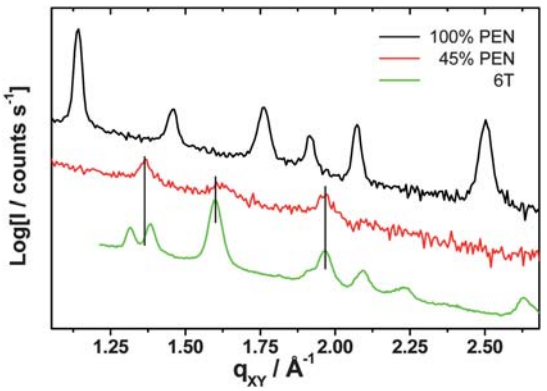

Fig. 24 In-plane XRD scans of 40 nm thick PEN/6T film.

presence of a mixed phase. The peak at q_z = 0.7968 Å^{-1} (d = 0.79 nm) might be associated with the (0 0 3) peak of the β-6T[43] phase and the (0 0 2) of the TF-PEN[27] phase.

The in-plane XRD scan (Fig. 24) clarifies the picture. No peaks related to PEN are observable in the co-deposited film spectra. The weak peaks at q_{xy} = 1.6167 Å^{-1} and q_{xy} = 1.9627 Å^{-1}of the co-deposited film can also be found in the 6T in-plane scan. A peak at q_{xy} = 1.3669 Å^{-1} is located between the peaks at 1.315 Å^{-1} and 1.383 Å^{-1} of the pure 6T film. We can deduce from the XRD measurement that a small part of the film has a periodicity similar to the 6T film. In contrast, no indication for ordered PEN can be found.

Since XRD probes only ordered portions of the sample with lattice planes oriented perpendicular and parallel to the substrate surface, we analyze the IR spectra of the γ(C–H) o.-o.-p. bending region of 6T and PEN (Fig. 25) to test for the presence of eventual unordered phases.

The films with low PEN content (30% and 45% PEN) (Fig. 25a) show a pronounced broadening of the peak at 729 cm^{-1} which has a similar line shape as in fully mixed PEN/4T films (Fig. 3) discussed earlier in this paper. This indicates that the local environment of the PEN molecules is very diverse. The 75% PEN film shows a superposition of the pure PEN film split-peak and the broad peak indicating a co-existence of ordered and amorphous phase. The PEN peak at 903.5 cm^{-1} doubles its line width and shows a blue shift of 1.8 cm^{-1} in the co-deposited films, partly due to the Christiansen effect.[47,48]

In contrast, the 6T γ(C–H) o.-o.-p. bending peaks (Fig. 25b) do not exhibit strong broadening. The Davidov splitting[37] of the γ(C$_α$–H) vibration around 688.7 cm^{-1} is still observable in all co-deposited films. The peak at 791.8 cm^{-1} shows almost no shift and no change of the line shape as it was observed for mixing material pairs like 6T/DH6T[13] and 6T/6P (Fig. 8). Both observations strongly indicate that most of the 6T molecules are in a phase very similar to that of the pure material film.

The IR data suggest that the film phase-separates into domains of amorphous PEN and ordered 6T. The XRD data shows that the 6T domains are not highly textured. A possible reason for the low order of the co-deposited film can be the rough substrate which the first two monolayers pose for the further deposited material. This rough substrate of the first layers prevents the following material from forming ordered layered structures.

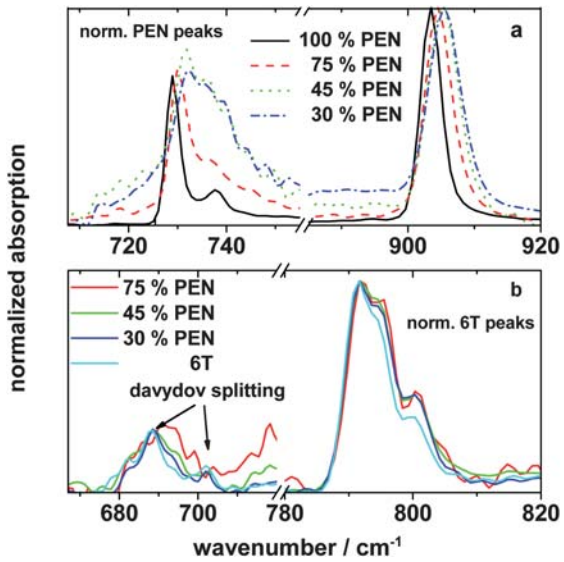

Fig. 25 IR spectra of 40 nm thick films grown SiO_2. γ(C–H) o.-o.-p. bending vibration peaks of PEN (a) and 6T (b) normalized to the peak maximum.

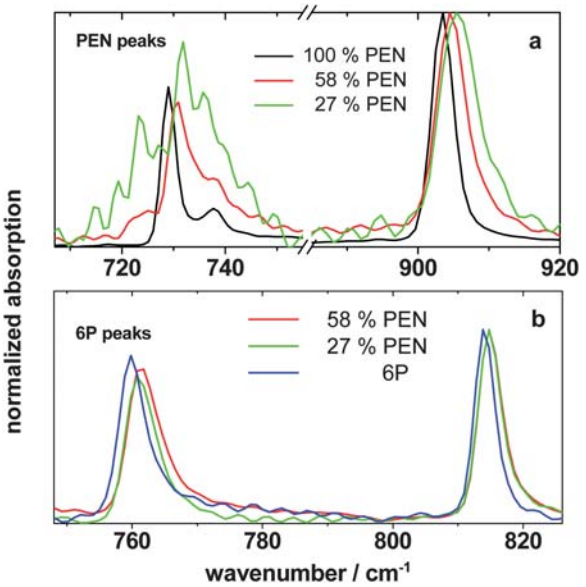

Fig. 27 IR spectra of PEN/6P films of 40nm thickness. γ(C–H) o.-o.-p. bending vibration peaks of (a) PEN and (b) 6P are normalized to the peak maximum.

3.8 Pentacene/*p*-sexiphenyl

The vdWLs of PEN[23] (1.64 nm) and 6P[40] (2.87 nm) differ by 1.2 nm (42%) therefore a similar morphology as observed for PEN/6T films could be expected and is actually observed. The AFM image of a 1.2 nm thick (sub monolayer) 49% PEN film is shown in (Fig. 26a). It exhibits loosely packed islands of about 3 nm height, which may indicate a phase separation of standing PEN and 6P domains on the few 10 nm scale. This layer (1.5 nm RMS roughness) forms a rough substrate for subsequent molecular layers. The 20 nm thick 46% PEN film (Fig. 26b) exhibits close-packed, needle-like, and about 70 nm high islands. This surface morphology with a RMS roughness of 16 nm to 20 nm does not significantly change (islands height, size, and shape) in the range of 70% to 27% PEN content. It has been reported that PEN grows in exactly this needle-like morphology, when deposited onto substrates with comparably rough surfaces, like polycrystalline gold films.[49]

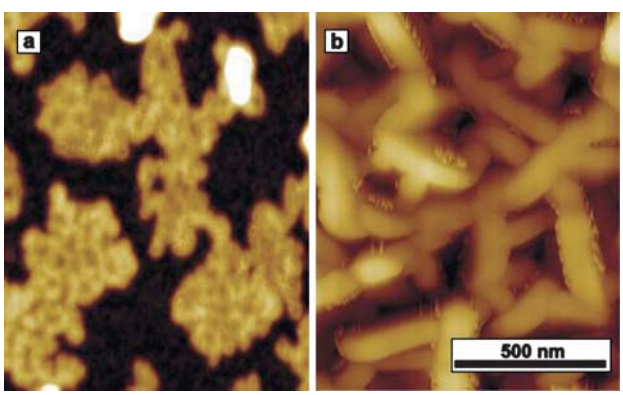

Fig. 26 AFM images of co-deposited PEN/6P films. (a) 49% PEN film of 1.2 nm thickness. (b) 20 nm thick 46% PEN film. The height of the needle-like structures ranges from 50 nm to 90 nm.

The IR spectra of the PEN γ(C–H) o.-o.-p. bending vibration region (Fig. 27a) give us information on the bulk properties of the film. The peaks at 729.1 cm^{-1} and 737.7 cm^{-1} are significantly broadened upon co-deposition with 6P. The main peak (729.1 cm^{-1}) shows a pronounced blue-shift of 1.7 cm^{-1} (58% PEN) and 2.4 cm^{-1} (27% PEN). (Note: The background intensity oscillation in the (27% PEN) spectrum is due to internal reflections in the sample and was amplified by the normalization procedure.) The peak at 903.4 cm^{-1} is blue-shifted by 2.1 cm^{-1} and its line width is almost doubled. This shifts can be partly attributed to the Christiansen[47,48] effect, since the surface corrugation of the co-deposited films (Fig. 27b) is significantly higher compared to the pure material films (*cf.* Fig. 2c, Fig. 5c), but the broadening and the loss of the line splitting clearly point towards an amorphous local environment of the PEN molecules.

On the other hand, the 6P γ(C–H) o.-o.-p. bending peaks (Fig. 27b) at 759.9 cm^{-1} and 814.2 cm^{-1} show only blue-shifts of 1.5 cm^{-1} and only 0.7 cm^{-1} due to the co-deposition of PEN. This shifts are small compared with the 3 cm^{-1} blue shifts observed for

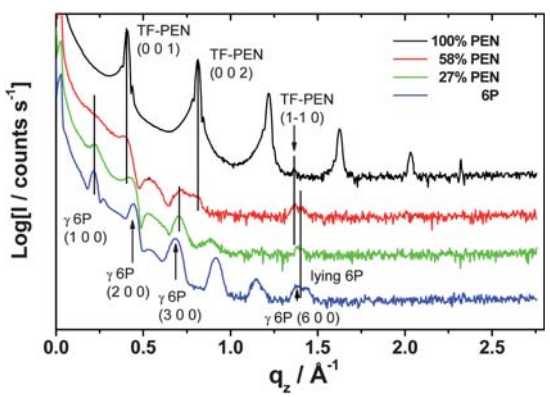

Fig. 28 Specular XRD scan of 40 nm thick PEN/6P films.

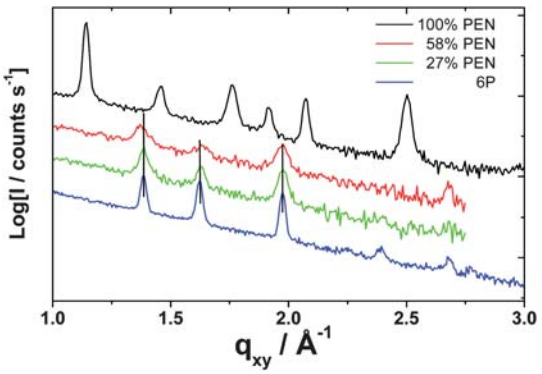

Fig. 29 In-plane XRD scans of 40 nm thick PEN/6P films.

the mixing material pair 6P/6T (*cf.* Fig. 8). The shift can be attributed to the Christiansen effect[47,48] caused by the high surface corrugation of the PEN/6P films. This indicates that the local environment of the 6P molecules is not changed in the co-deposited PEN/6P films and suggests a phase separation into ordered 6P domains and partly amorphous PEN domains.

The spatial order of the film was further studied *via* specular XRD (Fig. 28). The intensity of the (0 0 1) and (0 0 2) peak of the TF-PEN[27] phase, measured at $q_z = 0.4069$ Å^{-1} and $q_z = 0.8143$ Å^{-1} for the pure PEN film, decreases to ~1% of the original intensity for the 58% PEN film. This indicates that maximal 1% of the PEN in the co-deposited film has the orientation similar to the pure PEN film. In the 27% PEN film the TF-PEN (0 0 1) and (0 0 2) peaks are even not observable.

In contrast, the (1 0 0) peak of the γ-6P phase[44] exhibits in the co-deposited film (27% PEN/73% 6P film) 36% of the pure 6P film intensity. That means a large amount of the 6P molecules are in a similar orientation as in the pure 6P film. In the 58% PEN film the γ-6P (1 0 0) peak is very weak and broadened and the γ-6P (2 0 0) is superimposed with the TF-PEN (0 0 1) peak. The (300) peak of the γ-6P phase at $q_z = 0.6836$ Å^{-1} is shifted to $q_z = 0.7035$ Å^{-1} (27% PEN). This shift could be explained by a superposition with the β-6P (300) peak[44] with $d = 2.597$ nm and $q_z = 0.7258$ Å^{-1}. The broad peak at $q_z = 0.8837$ Å^{-1} can be associated with the (003) peak of bulk PEN[30] phase superimposed with the (400) γ-6P peak measured at 0.9164 Å^{-1}.

The peaks around $q_z = 1.394$ Å^{-1} are associated with PEN and 6P molecules with an orientation almost parallel to the substrate surface. The intensity of this peaks is slightly smaller than in the pure 6P film.

In contrast, the in-plane XRD scans show a much clearer picture (Fig. 29). The pure 6P film exhibit three major peaks at $q_{xy} = 1.3847$ Å^{-1}, $q_{xy} = 1.6231$ Å^{-1}, and $q_{xy} = 1.9741$ Å^{-1}. In the co-deposited films these peaks are only mildly broadened and exhibits shifts of below 0.004 Å^{-1}. On the other hand, none of the PEN film in-plane peaks could be observed in the spectra of the co-deposited films.

The co-deposition of PEN and 6P leads to films with needle-like surface morphology of high corrugation (16 nm–20 nm RMS roughness for 20 nm thick films). We attribute this growth mode to the roughness of the first molecular layer. This is hindering the subsequent molecules to grow in textured and well phase separated structures. The difference in the initial two layer seems to be the reason which separates the growth of PEN/6T and PEN/6P from the phase separating material pairs 4T/6T and 4T/6P which grow in well ordered and phase separated films.

Table 2 Phase separation and mixing between rod-like conjugated molecules in co-deposited thin films on silicon oxide. (vdWL: van der Waals length of the conjugated core)

	PEN (vdWL) (1.64 nm)	**4T** (1.82 nm)	**6T** (2.61 nm)	**6P** (2.87 nm)	**DH6T** (2.61 nm)
PEN		**Mixing**	Phase separation	Phase separation	Phase separation
4T			Phase separation	Phase separation	Phase separation
6T				**Mixing**	**Mixing**[a]
6P					**Mixing**[a]

[a] from ref. 13.

4.0 Summary

In this work we studied mixing and phase separation in co-deposited thin films of rod-like conjugated molecules. The results are compiled in Table 2.

Our results suggest the general rule that the co-deposition of rod-like conjugated molecules with CC of similar vdWL lead to the formation of films that exhibit intimate mixing of both materials on a molecular scale. A change of the total vdWL of one molecule by the attachment of alkyl end-chains does not lead to phase separation, *e.g.* DH6T/6P.

Co-deposition of materials with differently sized CC leads to phase separation. A striking difference in the growth mode between material pairs containing PEN and 4T was observed. Whereas 4T/6T and 4T/6P films show phase separation from the first layer on, the monolayer thick films of the PEN/6T and PEN/6P pairs exhibited mixing and phase separation on a few nm scale. This is attributed to stronger substrate-molecule interaction[50] for standing PEN molecules compared to standing 6T, 6P molecules, which expose one terminal hydrogen atom towards the substrate compared to two for PEN (Scheme 1). This may decrease the PEN diffusion length on the substrate and suppress phase separation on a larger length scale. The resulting rough monolayer film, consisting of domains on the 10 nm length scale, prevents the following molecular layers from forming highly ordered structures.

Overall, we demonstrated that it is possible to choose between phase separation and mixing by combining rod-like molecules with the appropriate CC sizes. This knowledge is of great value to find the right material combinations for applications like organic hetero-junction solar cells, where phase separation between donor and acceptor material is desired. Alternatively, hetero-films of organic semiconductors which show an intimate mixing, *e.g.* DH6T/6T, can be used as active layer in organic field effect transistor.

Acknowledgements

This work was supported by the Sfb448 (DFG). NK acknowledges financial support by the Emmy Noether Program (DFG), MO by the Austrian Science Foundation FWF-Project No. P21094. The authors thank W. Caliebe (HASYLAB, Hamburg, Germany) for experimental support.

Notes and references

1 W. Kuhlbrandt, *Structure*, 1995, **3**, 521.
2 J. P. Dekker and R. Van Grondelle, *Photosynth. Res.*, 2000, **63**, 195.
3 S. L. Wolfe, in *Molecular and Cellular Biology*, Wadsworth Publishing Company, 1993.
4 J. V. Barth, G. Costantini and K. Kern, *Nature*, 2005, **437**, 671.
5 F. Jackel, Z. Wang, M. D. Watson, K. Mullen and J. P. Rabe, *Synth. Met.*, 2004, **146**, 269.
6 B. P. Rand, J. Xue, S. Uchida and S. R. Forrest, *J. Appl. Phys.*, 2005, **98**, 124902.
7 F. Yang, M. Shtein and S. R. Forrest, *J. Appl. Phys.*, 2005, **98**, 014906.
8 P. Peumans, S. Uchida and S. R. Forrest, *Nature*, 2003, **425**, 158.
9 I. Salzmann, S. Duhm, R. Opitz, R. L. Johnson, J. P. Rabe and N. Koch, *J. Appl. Phys.*, 2008, **104**, 114518.
10 E. M. Han, L. M. Do, N. Yamamoto and M. Fujihira, *Thin Solid Films*, 1996, **273**, 202.
11 W. Porzio, U. Giovanella, M. Pasini, C. Botta, S. Destri and C. Provasi, *Thin Solid Films*, 2004, **466**, 231.
12 I. Salzmann, R. Opitz, S. Rogaschewski, J. P. Rabe, N. Koch and B. Nickel, *Phys. Rev. B: Condens. Matter Mater. Phys.*, 2007, **75**, 174108.
13 J.-O. Vogel, I. Salzmann, R. Opitz, S. Duhm, B. Nickel, J. P. Rabe and N. Koch, *J. Phys. Chem. B*, 2007, **111**, 14097.
14 P. Cosseddu, J.-O. Vogel, B. Fraboni, J. P. Rabe, N. Koch and A. Bonfiglio, *Adv. Mater.*, 2009, **21**, 344.
15 F. Garnier, G. Horowitz, X. H. Peng and D. Fichou, *Adv. Mater.*, 1990, **2**, 592.
16 D. Fichou, *J. Mater. Chem.*, 2000, **10**, 571.
17 F. Garnier, A. Yassar, R. Hajlaoui, G. Horowitz, F. Deloffre, B. Servet, S. Ries and P. Alnot, *J. Am. Chem. Soc.*, 1993, **115**, 8716.
18 A. Facchetti, M. Mushrush, M. H. Yoon, G. R. Hutchison, M. A. Ratner and T. J. Marks, *J. Am. Chem. Soc.*, 2004, **126**, 13859.
19 D. J. Gundlach, Y. Y. Lin, T. N. Jackson and D. G. Schlom, *Appl. Phys. Lett.*, 1997, **71**, 3853.
20 S. Duhm, H. Glowatzki, J. P. Rabe, N. Koch and R. L. Johnson, *Appl. Phys. Lett.*, 2006, **88**, 203109.
21 S. Tasch, C. Brandstätter, F. Meghdadi, G. Leising, G. Froyer and L. Athouel, *Adv. Mater.*, 1997, **9**, 33.
22 L. Antolini, G. Horowitz, F. Kouki and F. Garnier, *Adv. Mater.*, 1998, **10**, 382.
23 T. Siegrist, C. Kloc, J. H. Schon, B. Batlogg, R. C. Haddon, S. Berg and G. A. Thomas, *Angew. Chem., Int. Ed.*, 2001, **40**, 1732.
24 J. Ackermann, C. Videlot, P. Dumas, A. El Kassmi, R. Guglielmetti and V. Safarov, *Org. Electron.*, 2004, **5**, 213.
25 S. Zorba, Y. Shapir and Y. L. Gao, *Phys. Rev. B: Condens. Matter Mater. Phys.*, 2006, **74**, 245410.
26 T. Siegrist, C. Kloc, R. A. Laudise, H. E. Katz and R. C. Haddon, *Adv. Mater.*, 1998, **10**, 379.
27 C. D. Dimitrakopoulos, A. R. Brown and A. Pomp, *J. Appl. Phys.*, 1996, **80**, 2501.
28 A. C. Durr, F. Schreiber, M. Munch, N. Karl, B. Krause, V. Kruppa and H. Dosch, *Appl. Phys. Lett.*, 2002, **81**, 2276.
29 B. Warren, in *X-Ray diffraction*, Dover, 1990.
30 R. B. Campbell, J. Trotter and J. Monteath, *Acta Crystallogr.*, 1962, **15**, 289.
31 D. Nabok, P. Puschnig, C. Ambrosch-Draxl, O. Werzer, R. Resel and D. M. Smilgies, *Phys. Rev. B: Condens. Matter Mater. Phys.*, 2007, **76**, 235322.
32 S. Schiefer, M. Huth, A. Dobrinevski and B. Nickel, *J. Am. Chem. Soc.*, 2007, **129**, 10316.
33 H. Yoshida, K. Inaba and N. Sato, *Appl. Phys. Lett.*, 2007, **90**, 181930.
34 D. Holmes, S. Kumaraswamy, A. J. Matzger and K. P. C. Vollhardt, *Chem.–Eur. J.*, 1999, **5**, 3399.
35 T. Minakata, M. Ozaki and H. Imai, *J. Appl. Phys.*, 1993, **74**, 1079.
36 P. Hermet, J. L. Bantignies, A. Rahmani, J. L. Sauvajol and M. R. Johnson, *J. Phys. Chem. A*, 2005, **109**, 4202.
37 M. Kramer and V. Hoffman, *Opt. Mater.*, 1998, **9**, 65.
38 J. Lee, S. S. Kim, K. Kim, J. H. Kim and S. Im, *Appl. Phys. Lett.*, 2004, **84**, 1701.
39 T. Siegrist, R. M. Fleming, R. C. Haddon, R. A. Laudise, A. J. Lovinger, H. E. Katz, P. Bridenbaugh and D. D. Davis, *J. Mater. Res.*, 1995, **10**, 2170.
40 K. N. Baker, A. V. Fratini, T. Resch, H. C. Knachel, W. W. Adams, E. P. Socci and B. L. Farmer, *Polymer*, 1993, **34**, 1571.
41 E. Zojer, N. Koch, P. Puschnig, F. Meghdadi, A. Niko, R. Resel, C. Ambrosch-Draxl, M. Knupfer, J. Fink, J. L. Bredas and G. Leising, *Phys. Rev. B: Condens. Matter Mater. Phys.*, 2000, **61**, 16538.
42 G. Horowitz, B. Bachet, A. Yassar, P. Lang, F. Demanze, J. L. Fave and F. Garnier, *Chem. Mater.*, 1995, **7**, 1337.
43 B. Servet, G. Horowitz, S. Ries, O. Lagorsse, P. Alnot, A. Yassar, F. Deloffre, P. Srivastava, R. Hajlaoui, P. Lang and F. Garnier, *Chem. Mater.*, 1994, **6**, 1809.
44 R. Resel, N. Koch, F. Meghdadi, G. Leising, L. Athouel, G. Froyer and F. Hofer, *Cryst. Res. Technol.*, 2001, **36**, 47.
45 J. F. Fauvarque, M. A. Petit, A. Digua and G. Froyer, *Makromol. Chem.*, 1987, **188**, 1833.
46 G. Louarn, J. P. Buisson, S. Lefrant and D. Fichou, *J. Phys. Chem.*, 1995, **99**, 11399.
47 R. Prost, *Clays Clay Miner.*, 1973, **21**, 363.
48 M. Franz, B. M. Fischer and M. Walther, *Appl. Phys. Lett.*, 2008, **92**, 021107.
49 N. Koch, B. Nickel, J. Ghijsen, A. Elschner, J. Schwartz, J.-J. Pireaux and A. Kahn, *Mater. Res. Soc. Symp. Proc.*, 2003, **771**, L3.6.1.
50 S. Verlaak, S. Steudel, P. Heremans, D. Janssen and M. S. Deleuze, *Phys. Rev. B: Condens. Matter Mater. Phys.*, 2003, **68**, 195409.